Journal of Marine Science and Technology

Volume 21 | Issue 2 Article 12

AN IMPROVEMENT OF WAVE REFRACTION-DIFFRACTION EFFECT IN SWAN

aw-Guei Lin
Department of Harbor and River Engineering, National Taiwan Ocean University, Keelung, Taiwan, R.O.C.,
jglin@mail.ntou.edu.tw

Recommended Citation
Lin, aw-Guei (2013) "AN IMPROVEMENT OF WAVE REFRACTION-DIFFRACTION EFFECT IN SWAN," *Journal of Marine Science and Technology*: Vol. 21: Iss. 2, Article 12.
DOI: 10.6119/JMST-012-1207-1
Available at: https://jmstt.ntou.edu.tw/journal/vol21/iss2/12

AN IMPROVEMENT OF WAVE REFRACTION-DIFFRACTION EFFECT IN SWAN

Acknowledgements

This research was financially supported by the National Science Council under grant number NSC 97-2221-E-019- 047-MY3, Taiwan.

Journal of Marine Science and Technology, Vol. 21, No. 2, pp. 198-208 (2013)
DOI: 10.6119/JMST-012-1207-1

AN IMPROVEMENT OF WAVE REFRACTION-DIFFRACTION EFFECT IN SWAN

Jaw-Guei Lin

Key words: wave refraction-diffraction, SWAN, higher-order bottom slopes, wave-current interaction, rapidly varying sea bottom.

ABSTRACT

SWAN, a wind wave model, has been modified to take into account wave refraction-diffraction effects from the extended mild-slope equation when wind waves pass through a extremely uneven sea bottom in the presence of current. In our modified model, the diffraction correction parameter introduced by Holthuijsen *et al*. [10] has been adjusted to better predict the combined effect of the higher-order bottom effect, wave-bottom interaction and wave-current interaction. After a preliminary analysis, the influence of the correction parameter is discussed, and a comparison is made between the original and the new phase-decoupled versions of SWAN through some typical examples of wave fields around semi-infinite breakwaters, breakwaters with gap, and detached breakwaters on different bathymetries. The results show that the new phase-decoupled model exhibits improvements in both numerical convergence and Prediction results for the case of a steep varying an extremely uneven sea bottom than the original one.

I. INTRODUCTION

Wave prediction plays a very important role in human activities, whether on the ocean, near the shore, or along the coast by providing wave climate information under different weather conditions. For example, the safety of the navigation of commercial vehicles or yachts on open sea, the effective and safe transportation control of a harbor, searching or rescue of shipwreck, etc., are crucially dependent upon detailed and reliable information about the condition of the sea for decision making to ensure the safety of marine vehicles, cargo and crews. Also, because waves can become much larger in the nearshore zone, an accurate wave climate prediction will improve the safety of increasingly popular coastal recreation activities like yachting and surfing.

SWAN (Simulating Wave Nearshore), a third-generation wave model maintained by Delft University of Technology after Booij *et al*. [4], predicts waves' size and force by allowing for the changes of wave propagation from deep water to the surf zone. Nowadays it has become a very popular wind wave model, used by many government organizations, research institutes and consultant companies worldwide. As indicated in SWAN manuals [28, 29], the central responsibility of the model is to solve the spectral action balance equations which represent the effects of spatial propagation, refraction, shoaling, generation, dissipation and nonlinear wave-wave interactions, without any a priori restrictions on the spectral evolution of wind waves. However, the manual also points out that the the system has a weakness, as the diffraction effect is modeled in a restricted sense, so it is suggested that the resulting data only be used in areas where variations in wave height are large within a horizontal scale of a few wavelengths.

Within the last couple of decades, the refraction-diffraction problem has received a considerable amount of attention from coastal engineers and scholars, and a vast amount of research has been presented. For the phase-resolved models, Berkhoff [2] was something of a pioneer. Using linear wave theory, he derived a mild-slope equation (MSE) which served as a phase-resolved wave model to describe wave transformations from deep water to shallow water where there is a gradually varying sea bottom. Following this, many studies have been performed to extend the MSE to describe wave propagation over a rapidly varying seabed (e.g. Kirby [16]; Massel [22]; Chamberlain and Porter [6, 7]; Hsu and Wen [12, 13]; Liu [19]). The ability to compensate for the influence of ambient currents on the MSE using Luke's variation principle was given by Kirby [15] and Dingemans [8]. All quantities of the wavenumber $k(= 2\pi/L)$, the absolute wave angular frequency ω and the intrinsic wave angular frequency $\sigma(2\pi/T)$ are determined for a linear wave-current interaction system with the help of the dispersion relation $\sigma^2 = gk \tanh kh$, the Doppler-shift relation $\omega = \sigma + \boldsymbol{k} \cdot \boldsymbol{U}$, and the condition of irrotationality of the wavenumber vector $\nabla_h \times \boldsymbol{k} = 0$, where $\nabla_h = (\partial/\partial x, \partial/\partial y)$ is the horizontal gradient operator, $\boldsymbol{k}$ is the

Paper submitted 04/03/12; revised 09/02/12; accepted 12/07/12. Author for correspondence: Jaw-Guei Lin (e-mail: jglin@mail.ntou.edu.tw).
Department of Harbor and River Engineering, National Taiwan Ocean University, Keelung, Taiwan, R.O.C.

wavenumber vector and $\boldsymbol{U}$ is the current vector, L is the wavelength, and T is the wave period. Although there are many important contributors in this field, some other relevant research includes Smith and Sprinks [27], who used approximation theory to expand single frequency waves and thus obtain a parabolic mild-slope equation which greatly improved computational effectiveness, and Booij's [3] development of an elliptic mild-slope equation which takes into account the interaction of wave-currents by introducing current effects into traditional MSE via variational Lagrangian theory. In a similar move forward, Liu [18] expanded Smith and Sprinks [27] theory to calculate the interaction of vertical incident waves and jet flow on a sloping beach, and compared his results to the analytical solutions of Arthur [1].

Regarding phase-averaged models, SWAN (Booij *et al*. [5]; Ris *et al*. [24]), STWAVE (Steady-state spectral WAVE model) (Smith *et al*., [26]), TOMOWAC (Marcos, [20]) and WWM (Wind Wave Model) (Hsu *et al*., [11]) have been developed to compute the variation of wave spectra for short-crested random waves in large-scale oceanic deep water and in small-scale shallow water regions. Although these models readily attempt to account for the effects of refraction, a model which also handles wave diffraction has yet to be well implemented. Resio [23], Booij *et al*. [4] and Rivero *et al*. [25] tried to add wave diffraction into spectral models by introducing the diffraction effect in the propagation velocities via the modified wavenumber obtained from an energy balance equation of MSE, but their systems have not been widely accepted, and Mase [21] argues that their models seem to be unstable in their numerical calculations due to the higher-order spatial derivatives of the wave amplitude, and thus developed a simple and robust spectral model based on an energy balance equation combined with an energy dissipation term and a diffraction-correction term.

Holthuijsen *et al*. [10] have proposed an alternative that adds the wave diffraction effect obtained from MSE to the spectral model SWAN. This method is referred to as the phase-decoupled wave model. This model retains the ability to monitor all the physical processes of energy generation, dissipation and wave-wave interactions, but in addition to these, the specific tendencies of random waves is also incorporated into the model. Holthuijsen *et al*. [10] were the first to obtain a correction parameter δ_E which takes into consideration the directional tuning rates of the component waves induced by wave refraction and diffraction from MSE, where $\delta_E = \nabla_h \cdot (cc_g \nabla_h \sqrt{E}) / k^2 cc_g \sqrt{E}$, $c_g = nc$ is the wave group velocity, $n = (1 + 2kh/\sinh 2kh)/2$, c is the wave celerity, $E = \rho g a^2/2$ is the wave energy per unit width, ρ is the density of water, g is the gravitational acceleration, and a is the component wave amplitude. The correction parameter δ_E was used to modified the propagating velocities, c_x, c_y, c_σ and c_θ, in geometry space $x-$ and $y-$ and spectral space $\sigma-$ and $\theta-$ components, respectively, to improve the wave refraction and diffraction effects in the SWAN model. This model was compared with the multidirectional wave transformation around detached breakwaters by Ilic *et al*. [14] under different incident wave conditions which included factors of wind-sea, swell-sea and bimodal spectra. Good agreements were found through comparisons of model predictions and field observations for directional broad banded spectra.

The MSE used in the model of Holthuijsen *et al*. [10], however, is obtained under the assumption of the presence of linear gravity waves over a slowly varying seabed. In most coastal region, the topography is arbitrary and very complicated, abruptly varying topography like the edges of offshore or continental reefs or bars commonly appear on the sea bottom. For these reasons this model is of limited applicability in real world scenarios. Furthermore, there usually exists an ambient current field due to the gradient of driving forces such as the wind-shear stress, attractive, Coriolis force, hydrostatic forces and so on. These phenomena are also not included in the MSE applied by Holthuijsen *et al*. [10].

In this paper, correction parameters obtained from MSE, including the higher-order bottom slope terms and ambient current effects, are introduced into SWAN. The wave action equation is adjusted to include refraction and diffraction-induced directional tuning rate of component waves. Similar work has been done on a WWM model by Liau *et al*. [17], but their model is written in finite element method (FEM) and has not yet been done in SWAN. The extension of wave refraction, diffraction and reflection in SWAN is able to give more accurate results and can be applied in most situations with rapidly varying topography where wave diffraction is a dominant feature. In the following sections, the derivation of an extended mild-slope equation is first introduced followed by a description of the modification of a wave action baance equation. A key feature of the approach used in this study is that we are able to evaluate the relative importance of the higher-order terms of steep slopes, curvatures and wave-current interactions that influence wave diffraction. Several computational cases with waves traveling over an abruptly varying topography or in current fields have been performed to validate the proposed model.

II. THE EXTENDED MILD-SLOPE EQUATION (EMSE)

The bit stream to be transmitted is organized in frames as shown in Fig. 1. The preamble and the end code indicate the start and the end of a message frame, respectively. They are used by the receiver for the frame synchronization. The training sequence is used by the adaptive equalizer in the receiver for optimizing the equalizer coefficients. The information-bearing data follow the training sequence. The gap between the preamble and the training sequence is for ensuring the completion of the frame synchronization in the receiver before the reception of the training sequence.

Considering the second-order bottom effects with bottom curvature $\nabla_h^2 h$ and bottom slope $|\nabla_h h|$, and the influence of

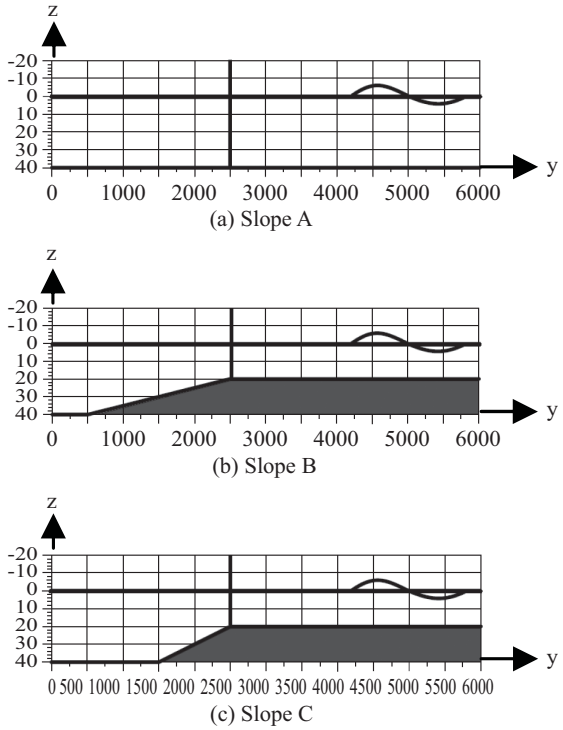

Fig. 1. Three different bathymetries for simulations.

ambient current fields, the extended MSE (EMSE) given by Liu (1990) is written in the form

$$\begin{aligned}&\nabla_h\cdot\left(cc_g\nabla_h\phi\right)+k^2cc_g\phi+\left(f_1g\nabla_h^2h+f_2gk\left|\nabla_h h^2\right|\right)\phi\\&\quad+i\omega\left[\boldsymbol{U}\cdot\nabla_h\phi+\nabla_h\cdot(\boldsymbol{U}\phi)\right]-\left(\sigma^2-\omega^2\right)\phi\\&=\nabla_h\cdot\left[\boldsymbol{U}\left(\boldsymbol{U}\cdot\nabla_h\phi\right)\right]\end{aligned}\tag{1}$$

where ϕ is the velocity potential given by

$$\phi=\phi(x,y,z;t)=\frac{iga(x,y;t)}{\sigma}\frac{\cosh k\left(z+h\right)}{\cosh kh}e^{iS(x,y;t)}\tag{2}$$

$S(x, y; t)$ is the phase function; $i=\sqrt{-1}$ is the unit complex number; $h(x, y; t)$ is the water depth related to free water surface. The Doppler-shift relation between the absolute and intrinsic angular frequency for linear wave-current coexisting system is given by

$$\omega=\sigma+\boldsymbol{k}\cdot\boldsymbol{U}=\sigma+k\cos\theta U_x+k\sin\theta U_y=\sigma+kU_S\tag{3}$$

where $\boldsymbol{k}=(k\cos\theta, k\sin\theta)$; θ is the wave angle; $U_S=U_x\cos\theta+U_y\sin\theta$ denotes the dot product between the ambient current velocity and the unit wavenumber vector along the wave propagation direction; f_1 and f_2 are functions of relative water depth, respectively expressed as

$$\begin{aligned}f_1=&\frac{-4kh\cosh kh+\sinh 3kh+\sinh kh+8(kh)^2\sinh kh}{8\cosh^3 kh(2kh+\sinh 2kh)}\\&-\frac{kh\tanh kh}{2\cosh^2 kh}\end{aligned}\tag{4}$$

$$\begin{aligned}f_2=&\frac{\operatorname{sech}^2kh\left[8(kh)^4+16(kh)^3\sinh 2kh-9\sinh^2 kh\cosh 2kh\right]}{6(2kh+\sinh 2kh)^3}\\&+\frac{12(kh)(1+2\sinh^4 kh)(kh+\sinh 2kh)}{6(2kh+\sinh 2kh)^3}\end{aligned}\tag{5}$$

Detailed derivation of Eq. (1) can be found in Liu [19].

Upon substituting Eq. (2) into Eq. (1), we obtain the real part and imaginary part. The real part is

$$\begin{aligned}&\nabla_h\left(cc_g\right)\cdot\nabla_h a+cc_g\left(\nabla_h^2a-a\left(\nabla_h S\right)^2\right)+k^2cc_g a\\&\quad+a\left(f_1g\nabla_h^2h+f_2gk\left|\nabla_h h\right|^2\right)\\&\quad-2a\omega\boldsymbol{U}\cdot\nabla_h S-a(\sigma^2-\omega^2)\\&=2\boldsymbol{U}\nabla_h\boldsymbol{U}\cdot\nabla_h a+\boldsymbol{U}^2\cdot\left(\nabla_h^2a-a\left(\nabla_h S\right)^2\right)\end{aligned}\tag{6}$$

and the imaginary part is

$$\begin{aligned}&a\nabla_h\left(cc_g\right)\cdot\nabla_h S+cc_g\left(2\nabla_h a\cdot\nabla_h S+a\nabla_h^2S\right)\\&\quad+\omega[2\boldsymbol{U}\cdot\nabla_h a+a\nabla_h\boldsymbol{U}]\\&=2a\boldsymbol{U}\nabla_h\boldsymbol{U}\cdot\nabla_h S+\boldsymbol{2U}^2\cdot\nabla_h a\cdot\nabla_h S+a\boldsymbol{U}^2\cdot\nabla_h^2S\end{aligned}\tag{7}$$

Eq. (6) uses the eikonal equation due to the wave diffraction effect, that is

$$\begin{aligned}K^2=&\left|\nabla_h S\right|^2\\=&k^2+\frac{\nabla_h\cdot\left(cc_g\nabla_h a\right)}{cc_g a}+f_1\frac{g\nabla_h^2h}{cc_g}+f_2\frac{gk\left|\nabla_h h\right|^2}{cc_g}\\&+\frac{\left(\omega-\boldsymbol{U}\cdot\nabla_h S\right)^2}{cc_g}-\frac{\sigma^2}{cc_g}-\frac{\nabla_h\cdot\left[\boldsymbol{U}\left(\boldsymbol{U}\cdot\nabla_h a\right)\right]}{cc_g a}\end{aligned}\tag{8}$$

where K is the wavenumber caused by the combined refraction and diffraction effects of the horizontal variation of the wave amplitude, bathymetry configuration and current field. More detailed derivation of Eq. (8) can be found in Liau *et al*. [17].

By substituting Eq. (3) into Eq. (8) and introducing a refraction-diffraction correction parameter $\overline{\delta}$ may be more accurately expressed as

$$\bar{\delta} = \frac{(c+U_s)U_s - \sqrt{\left[(c+U_s)U_s\right]^2 - \left[\left(cc_g\right)U_s{}^2 - \left(cc_g\right)^2\right]\delta_N}}{\left(U_s{}^2 - cc_g\right)} \tag{9}$$

where δ_N is a parameter including the effect of current and is written as

$$\delta_N = 1 + \frac{1}{k^2 cc_g a}\left[\nabla_h \cdot \left(cc_g \nabla_h a\right) - \nabla_h \cdot \left(U_s{}^2 \nabla_h a\right)\right] + \frac{1}{k^2 cc_g}\left[f_1 g\nabla_h^2 h + f_2 gk\left|\nabla_h h\right|^2\right] + \frac{1}{n}\left(\frac{U_s}{c}\right)\left(2 + \frac{U_s}{c}\right) \tag{10}$$

The relation between the new wavenumber K with wave diffraction effect and the wavenumber k is then shown as

$$K = \bar{\delta} k \tag{11}$$

Liau *et al*. [17] state that the EMSE used in the present model is only valid for propagating waves. The mathematical formulation didn't take non-propagating (evanescent) modes into account. Therefore, K is not realistic if the square root is imaginary. When neglecting the effects of rapidly varying sea bottom and of ambient current field, Eq. (11) is readily reduced to the eikonal equation provided by Holthuijsen *et al*. [10], i.e.

$$K = k\delta_m = k\left[1 + \frac{\nabla_h (cc_g \nabla_h a)}{k^2 cc_g a}\right]^{0.5} \tag{12}$$

where δ_m is the refraction-diffraction correction parameter obtained from conventional MSE. Holthuijsen *et al*. [10] has shown that the parameter δ_m allows for the diffraction-induced directional turning rate in the SWAN model (Booij *et al*. [5]).

According to Eq. (11), the diffraction-correction phase speed C can be obtained as follows.

$$C = \frac{\omega}{K} = \frac{c + U_s}{\bar{\delta}} \tag{13}$$

The imaginary part in Eq. (7) leads to the energy transport equation after multiplying the wave amplitude a:

$$\nabla_h \cdot \left\{ \left[cc_g \nabla_h S + (\omega - \boldsymbol{U} \cdot \nabla_h S)\boldsymbol{U}\right] a^2 \right\} = 0 \tag{14}$$

By using the relations of $\boldsymbol{K} = \nabla_h S$, $K = k\bar{\delta}$ and $c = \sigma/k$, Eq. (14) is in terms of the energy transport equation given by

$$\nabla_h \cdot \left\{ \left[\bar{\delta} c_g + \left(1 + \left(\frac{U_s}{c}\right)(1 - \bar{\delta})\right)\boldsymbol{U} \right] a^2 \right\} = \nabla_h \cdot \left\{\boldsymbol{C}_g E\right\} = 0 \tag{15}$$

It can be seen that a modified wave propagation velocity with current effect is represented by the conventional wave energy conservation equation. Therefore, the energy propagation speed due to the diffraction effect in geographic space is written as

$$\boldsymbol{C}_g = \bar{\delta}\boldsymbol{c_g} + \left[1 + \left(\frac{U_s}{c}\right)\left(1 - \bar{\delta}\right)\right]\boldsymbol{U} \tag{16}$$

where $\boldsymbol{C}_g = (C_x, C_y)$, C_x and C_y are the wave energy propagation velocity components due to diffraction with current and rapidly varying bottom effects in the x- and y- directions, respectively. Under the absence of currents and higher-order bottom effects, Eq. (16) is reduced to $\boldsymbol{C_g} = \delta_m \boldsymbol{c_g}$ which is identical to equation from the theory of Holthuijsen *et al*. [10].

III. MODIFICATION OF WAVE ACTION BALANCE EQUATION

In SWAN model, the evolution of the wave spectrum is described by the wave action balance equation (e.g., Hasselmann *et al*. [9]). The equation expressed by Cartesian coordinates is

$$\frac{\partial N}{\partial t} + \frac{\partial}{\partial x}(c_x N) + \frac{\partial}{\partial y}(c_y N) + \frac{\partial}{\partial \sigma}(c_\sigma N) + \frac{\partial}{\partial \theta}(c_\theta N) = \frac{S_{total}}{\sigma} \tag{17}$$

where $N = N(\sigma, \theta)$ is the wave action density spectrum; t is time; c_x, c_y, c_σ and c_θ are the wave propagation velocities in $x-$, $y-$, $\sigma-$ and $\theta-$ components, respectively; the right hand side term S_{total}/σ is the source term in terms of energy density representing the processes of wave energy generation, dissipation and redistribution.

With the aid of correction parameter $\bar{\delta}$, the wave refraction-diffraction effect can be added to the wave action balance equation, and the corresponding propagation speeds c_x, c_y, c_σ and c_θ are replaced by C_x, C_y, C_σ and C_θ. The resulting expressions for the propagation speeds in the geographic and spectral spaces are given, respectively, by

$$C_x = C_g \cos\theta = \bar{\delta} c_g \cos\theta + [1 + (\frac{U_S}{c})(1 - \bar{\delta})]U_x \tag{18}$$

$$C_y = C_g \sin\theta = \bar{\delta} c_g \sin\theta + [1 + (\frac{U_S}{c})(1 - \bar{\delta})]U_y \tag{19}$$

$$C_\sigma = \frac{\partial \sigma}{\partial h}\left[\frac{\partial h}{\partial t} + U_x \frac{\partial h}{\partial x} + U_y \frac{\partial h}{\partial y}\right] - \bar{\delta} c_g k(\cos\theta \frac{\partial U_s}{\partial x} + \sin\theta \frac{\partial U_s}{\partial y}) \tag{20}$$

$$C_\theta = \overline{\delta} c_g \left[\frac{1}{k}(\sin\theta \frac{\partial k}{\partial x} - \cos\theta \frac{\partial k}{\partial y}) + \frac{1}{\overline{\delta}}(\sin\theta \frac{\partial \overline{\delta}}{\partial x} - \cos\theta \frac{\partial \overline{\delta}}{\partial y}) \right]$$
$$+ (\sin\theta \frac{\partial U_s}{\partial x} - \cos\theta \frac{\partial U_s}{\partial y}) \quad (21)$$

Referring to Eqs. (9) and (10), we notice that $\overline{\delta}$ contains the combined effects of a, $|\nabla_h h|$, $\nabla_h^2 h$ and U_s. Although the diffraction of short-crested random waves can be calculated as the superposition of refraction-diffraction effects of a number of incident monochromatic waves with different directions, such a method is impractical in the wave spectral model because of the problems with certain physical properties, such as an ignorance of wave-wave interaction as well as numerical convergence. For computational convenience in the SWAN model, as suggested by Holthuijsen *et al*. [10], it is plausible to express the wave amplitude a in Eq. (10) using the square root of the summation of wave action densities, that is

$$a = \sqrt{2E/\rho g} = \sqrt{2/\rho g} \sqrt{\sum_{i=1}^{I}\sum_{j=1}^{J} \sigma_{i,j} N(\sigma_i, \theta_j) d\theta d\sigma} \quad (22)$$

where I and J denote the total numbers of components in the wave frequency and direction spaces, respectively.

By introducing the parameter $\overline{\delta}$, Eqs. (9) and (10), into Eqs. (18) to (21) of the directional turning rate of wave propagation velocities, the modified action balance equation shows that the phase-decoupled approximation can take into account the wave refraction, diffraction and the reflection of random waves on an arbitrary bathymetry in the presence of an ambient current.

In SWAN source code, the related subprograms for modification are SWCOMP and SWOMPU in swancom1.for, DIFPAR, SWAPAR, SPROXY and SPROSD in swancom5.for, and KSCIP1 in swanser.for.

IV. COMPARISONS

As mentioned above, the main purpose of adding the phase-decoupled refraction-diffraction approximation to the wave action balance equation is to obtain a reasonable estimate of wave diffraction in the computations of SWAN, especially for those cases with rapidly varying sea bottoms in which there is an ambient current. The verification of the present model by field observations is difficult, however, as only a few small-scale numerical simulations and hydraulic model tests by previous researchers under the long-crested wave conditions are available. In this paper, we will compare the numerical results from SWAN ver. 40.72 and the new version modified in this study to seek the benefits of adding the refraction-diffraction effect in SWAN.

In this section, as the side views show in Fig. 1, three

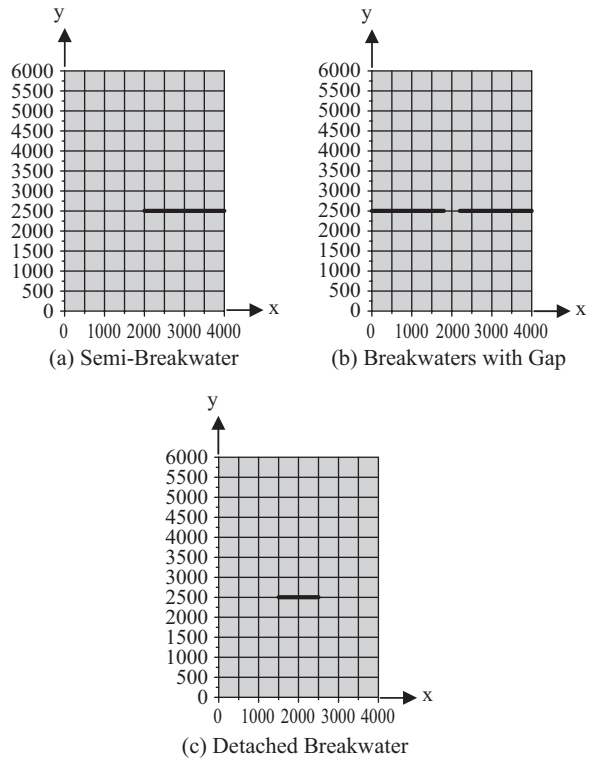

Fig. 2. Three types of layout for simulations.

different uniform sea bottoms with different constant slopes were used to observe the influence of sea bottom slope. Three layouts (a semi-breakwater, breakwaters with gap of 200 m, and a detached breakwater of 1000 m long) were used in the comparisons of original version and new version of the SWAN models. Fig. 2 shows the plain view of the layouts. In SWAN simulations, the computational domain is set at 4000 m × 6000 m with a grid size of 10 m × 10 m. The JONSWAP spectral parameter γ is 3.3, and directional spreading parameter was selected to be 2 for short-crested random waves and 50 for long-crested random waves.

In the following discussion of different layouts situated at different bathymetries, the K_D profiles at x = 2000 m have been plotted for evaluation. The cases with wave period T_S = 6 s, 8 s, and 10 s are compared. In each figure, the left column presents the results from the original version, and the right column presents the results from new version. The results of three bathymetries have been plotted in each plot. Some K_D contour results in different layouts on Slope C for wave period of T_S = 8 s are shown for the evaluation of the numerical differences.

1. Semi-Infinite Breakwater

For the cases of a semi-infinite breakwater situated at different bathymetries, Figs. 3 and 4 show the K_D profiles when x = 2000 m for three different bathymetries. Fig. 3 shows those for short-crested cases and Fig. 4 shows the long-crested random wave cases. For short-crested random wave cases,

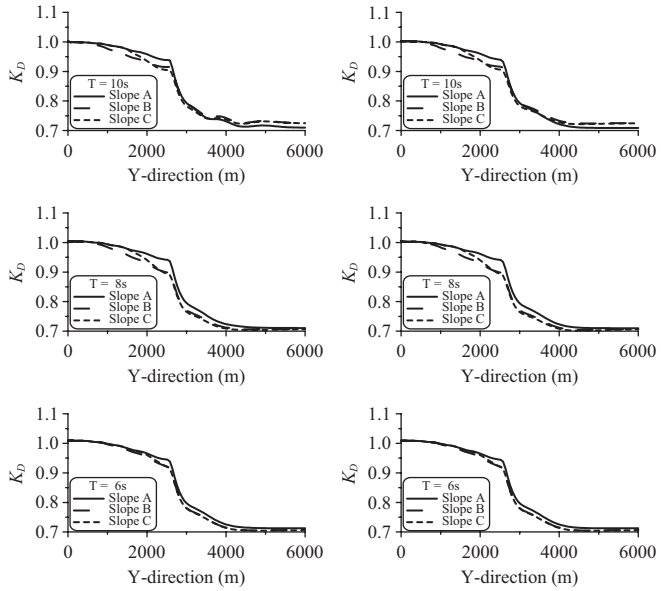

Fig. 3. K_D profiles at x = 2000 m for semi-infinite breakwater in short-crested random wave cases.

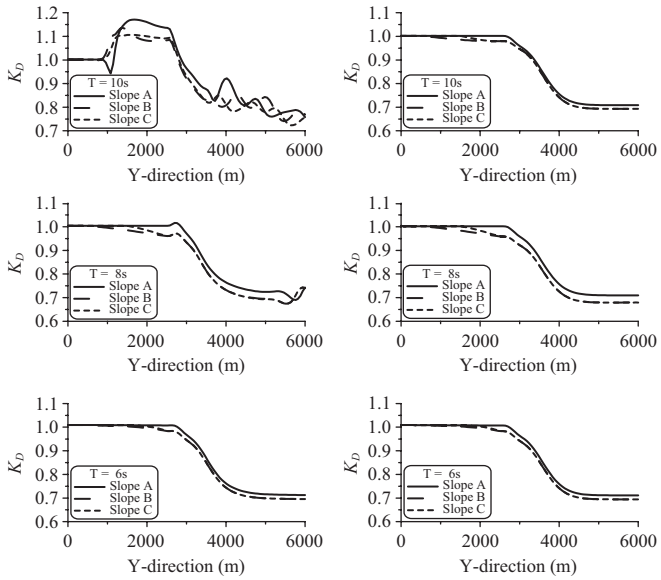

Fig. 4. K_D profiles at x = 2000 m for semi-infinite breakwater in long-crested random wave cases.

due to the incident waves are directional spreading, the directly incident waves approach from the left hand side of the figures to the inner water behind the breakwater, and reduces the influence of diffraction; in these cases the wave height distributions are similar, but with slight differences. However, for long-crested random wave cases, the numerical results have varied greatly as the incident wave periods become longer. Fig. 5 shows the K_D contours on Slope C. Some numerical instability occurs on the left hand side behind the breakwater in the original SWAN version, however, the modified version fixed the problem.

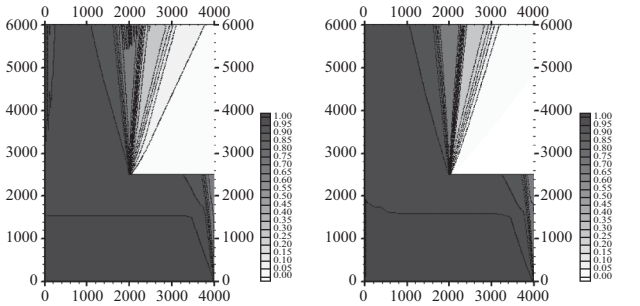

Fig. 5. K_D contours around semi-infinite breakwater on Slope C in long-crested random wave cases (wave period T_S = 8 s).

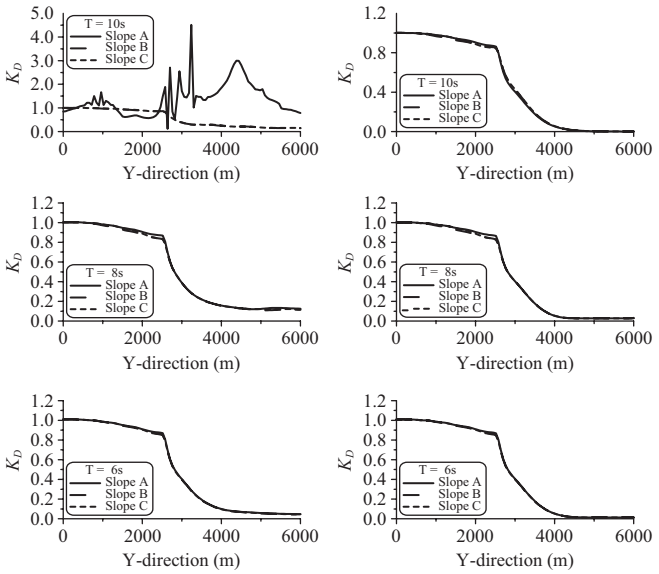

Fig. 6. K_D profiles at x = 2000 m for breakwaters with gap in short-crested random wave cases.

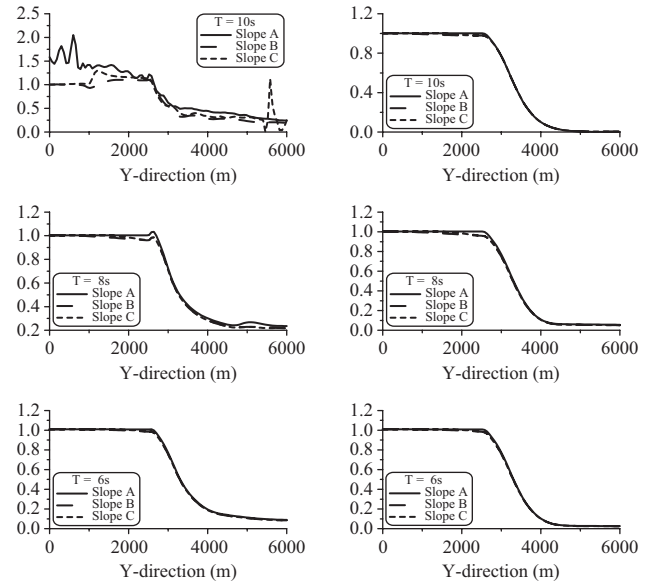

Fig. 7. K_D profiles at x = 2000 m for breakwaters with gap in long-crested random wave cases.

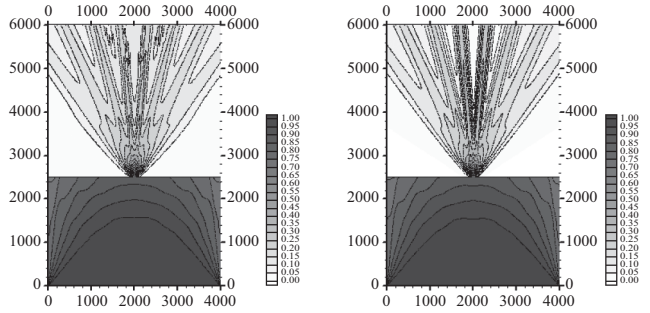

Fig. 8. K_D contours around breakwaters with gap on Slope C in short-crested random wave cases (wave period T_S = 8 s).

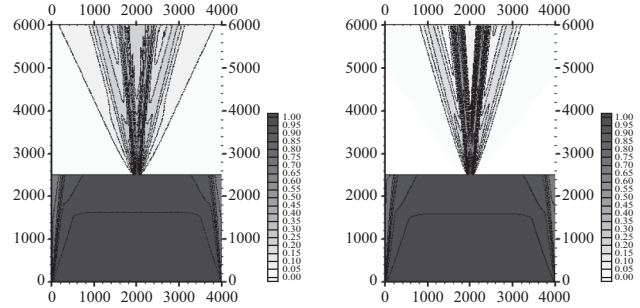

Fig. 9. K_D contours around breakwaters with gap on Slope C in long-crested random wave cases (wave period T_S = 8 s).

2. Breakwaters with Gap

For breakwaters with gap, Figs. 6 and 7 show the K_D profiles at x = 2000 m. For the wave periods discussed in these figures, T_S = 6 s, 8 s, and 10 s, the related wavelengths at the entrance are 55 m, 88.8 m and 121.2 m, respectively, which means that the incident wavelengths of wave periods of 6 s and 8 s are shorter than the gap width, but when the wavelength of T_S = 10 s is greater than the gap width, the diffraction effects might be different.

Figs. 8 and 9 show the K_D contours, by comparing the numerical results between these two figures, since the short-crested wave cases are directional spreading, one can find that the diffracted waves behind the breakwaters spread more broadly in short-crested random wave cases than in the cases of long-crested waves. The numerical instabilities can also be seen in the left columns of Figs. 6 and 7 for the original SWAN version. In Figs. 8 and 9, we can find that when the wavelengths are greater than the width of opening, the original SWAN version cannot properly predict the wave condition around the breakwater. However, in the new version, this problem is seems to be solved, and satisfactory predictions are generated.

3. Detached Breakwater

The simulations of wave fields adjacent to a 1 km long detached breakwater situated at different bathymetries are evaluated in this section. Figs. 10 and 11 show the K_D profiles for x = 2000 m. For long-crested wave cases, shown in Fig. 11, the numerical instability can be seen in original version, and it can also be seen that the new version improves the problem. However, such problem cannot be seen in Fig. 10 due to the broad directional spreading in short-crested wave cases; the waves directly propagate from two sides of the detached breakwater and reduce the diffraction effects of normal incident waves. The wave height distributions of the two SWAN versions behind the breakwater have little difference but are all stable. Figs. 12 and 13 show the results of

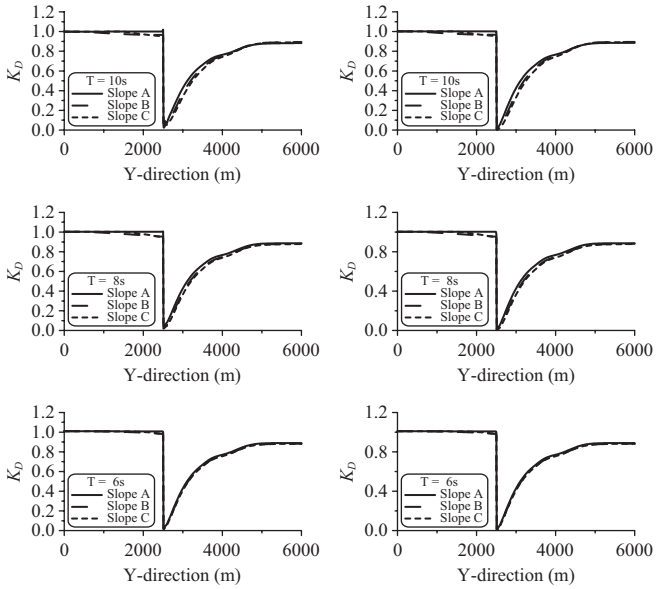

Fig. 10. K_D profiles at x = 2000 m for a detached breakwater in short-crested random wave cases.

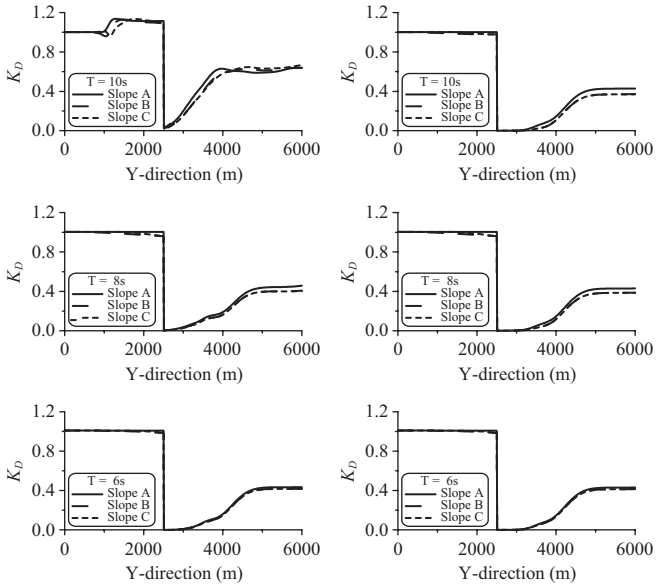

Fig. 11. K_D profiles at x = 2000 m for a detached breakwater in long-crested random wave cases.

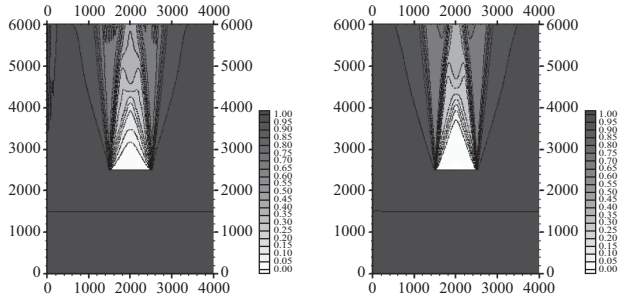

Fig. 12. K_D contours around a detached breakwater on Slope C in long-crested random wave cases (wave period T_S = 8 s).

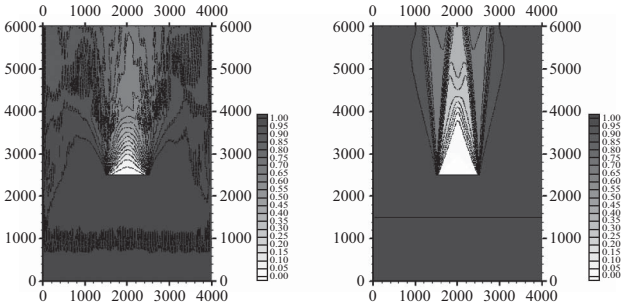

Fig. 13. K_D contours around a detached breakwater on Slope C in long-crested random wave cases (wave period T_S = 10 s).

long-crested random wave cases of T_S = 8 s and 10 s, respectively. It can be seen that the longer the wave period, the stronger the numerical instability in the original SWAN version, although this is not the case in new version.

V. COMPARISONS BETWEEN TWO VERSIONS OF SWAN

In order to find the difference between two versions of SWAN, Figs. 14 to 16 compare two models' K_D profiles at x = 2000 m for three layouts positioned on three bathymetries. In each figure, the left column presents long-crested random wave cases and the right column presents short-crested random waves cases. Within each plot in the figures, the results of both the original version and the new versions of SWAN are plotted for comparison purposes. As discussed earlier, the wave refraction-diffraction effect is affected by the bathymetry and the directional spreading of incident waves. In semi-infinite breakwater cases, as shown in Fig. 14, the diffraction effect can be covered by directly propagating waves from the open water zone beside the breakwater due to the broad spreading of wave directions. The results of the two versions are almost the same in the short-crested random wave cases. When the wave directional spreading is narrow, such as in long-crested random wave cases, the diffraction effect induced by the change of bathymetry plays a significant role. Great differences between the two versions appear in long wave period cases. Because the breakwaters with a gap have a stronger diffraction effect than the other two

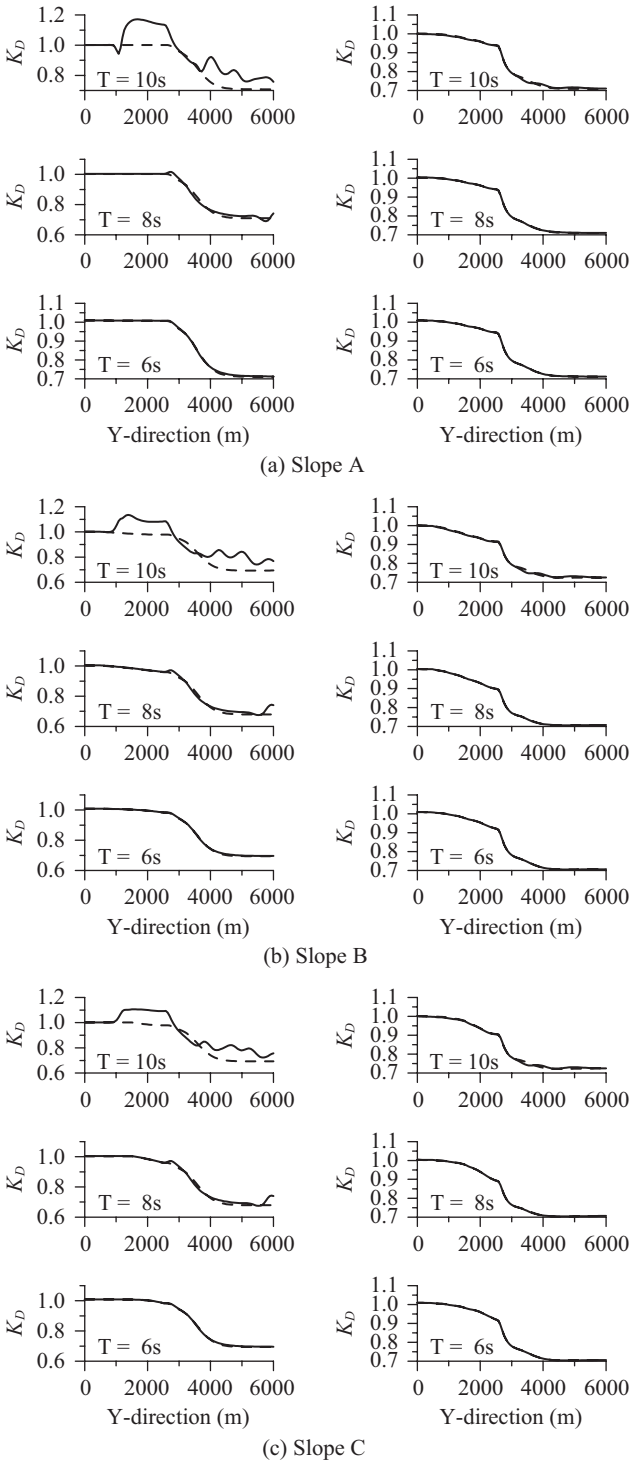

Fig. 14. Comparisons of K_D profiles at x = 2000 m for semi-infinite breakwater.

layouts, the two models have great differences in all wave cases, especially when the wavelength is longer than the opening width, as we can see in Fig. 15. In the detached breakwater cases, as shown in Fig. 16, a huge number of waves directly propagate from both sides of the breakwater. The two versions have almost the same results in short-crested

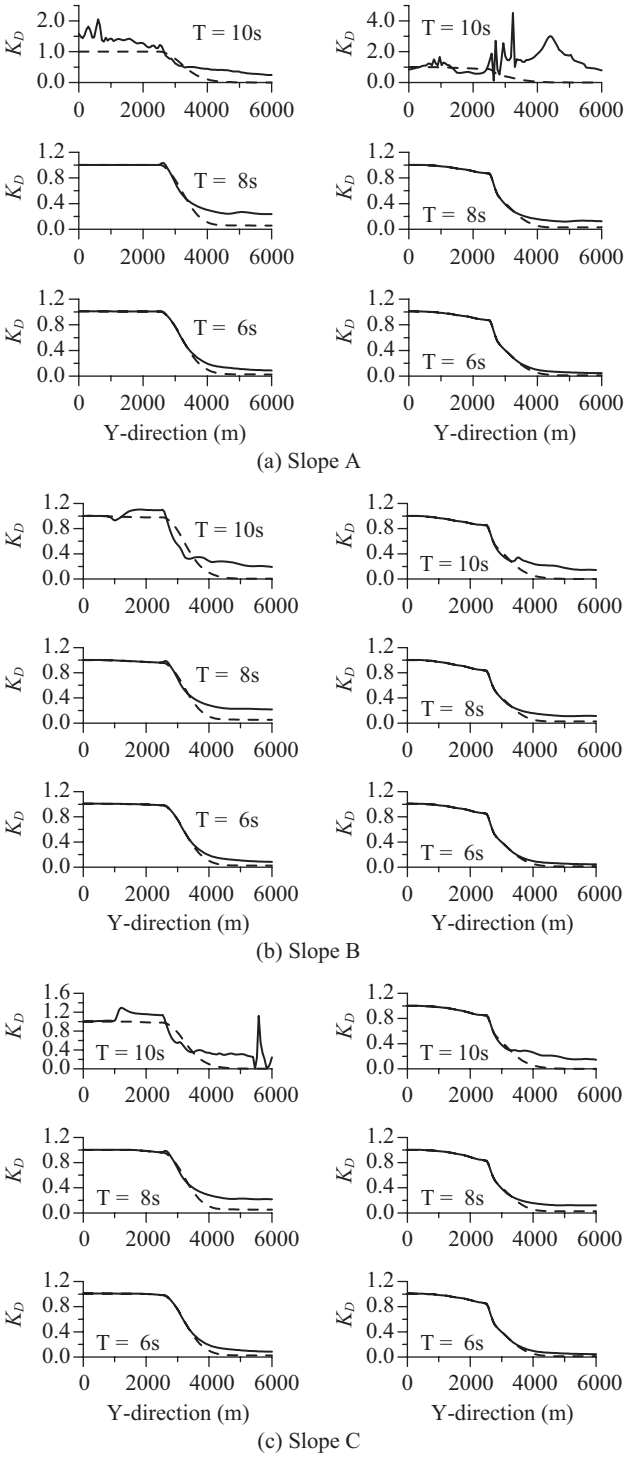

Fig. 15. Comparisons of K_D profiles at x = 2000 m for breakwaters with gap.

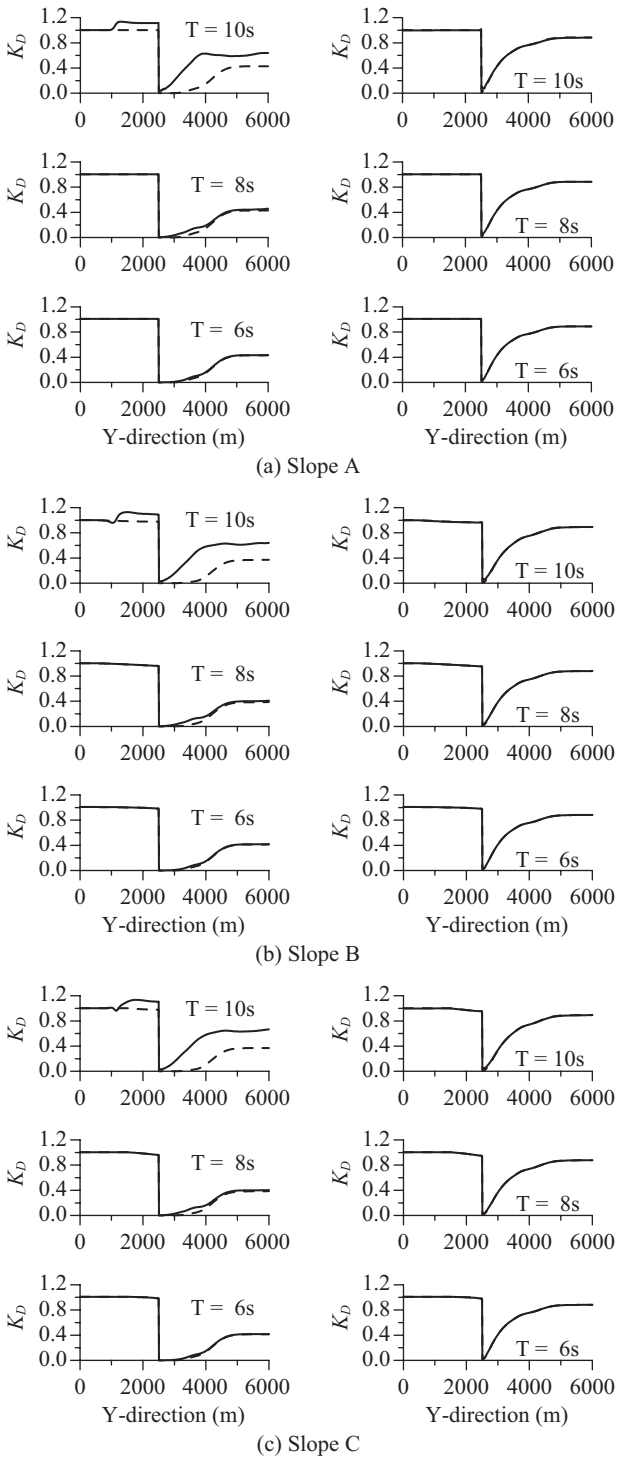

Fig. 16. Comparisons of K_D profiles at x = 2000 m for a detached breakwater.

random wave cases, however, in long-crested random wave cases, the difference between the two versions increases the when relative water depth becomes shallower when there are long period waves, a situation which causes the refraction-diffraction effect to get stronger.

After studying the comparisons, it is clear that the new version of SWAN shows its benefits in the field of wave predictions. It overcomes the numerical instability in the original version in environments where the sea bottom changes rapidly, or when the refraction-diffraction effect becomes stronger, or in situations in which the bandwidth of the wave spectrum is narrows.

VI. DISCUSSION

In long-crested random wave cases, the wave refraction-diffraction effect has a strong influence on the wave conditions behind the structures. The original SWAN has been found to be numerically unstable in such cases in all studied layouts (e.g. T_S = 10 s cases in this paper) and the new version improves the situation. When the wave refraction-diffraction effect becomes weaker, the results in both versions become identical (e.g. T_S = 6 s cases in this paper).

In short-crested random wave cases, due to the broader directional spreading, waves propagating in different directions might compensate for the wave fields behind the structure. The numerical results in both versions have slight difference in our cases when the wave refraction-diffraction effect is weak. For example, in semi-infinite breakwater cases and in detached breakwater cases, the structures are surrounded by an open water zone. Many waves can propagate to the back of structures without diffraction, and thus weaken the diffraction effect in the final results. In those cases involving breakwaters with gaps, however, the diffraction effect on the wave conditions behind the breakwaters is strong, and the numerical instability influences the results when the incident wavelength is greater than the gap width (e.g. T_S = 10 s cases in this paper) in the original SWAN, but the new version of SWAN improves the problem.

In practice, short-crested random waves mostly exist in ordinary weather where the wave conditions relate to human activities near the shore and along the coast. On the other hand, long-crested random waves always appear in severe weather like typhoon conditions or in the heart of the monsoon season when there are large wave heights and long periods in dominant directions, which are the major concerns in engineering planning/design, and in coastal/port management. Therefore, both wave cases are important. The new versions can offer a better approximation than the original SWAN.

VII. CONCLUSION

By adding the refraction-diffraction correction parameter $\overline{\delta}$, which incorporates the second-order bottom effects with bottom curvature $\nabla_h{}^2 h$ and bottom slope $\left|\nabla_h h\right|$, and the influence of ambient current fields based on extended mild-slope equation (Liu, 1983), into the earlier SWAN model, we have developed an improved model. A phase-decoupled refraction-diffraction approximation for waves propagating over a rapidly varying topography with an ambient current for the spectral wave model has been developed in this study. From the above comparisons between the original SWAN and this new version of SWAN, it can be seen that the new correction parameters improve the numerical instability of the original version for waves adjacent to a coastal structure positioned on a rapidly varying sea bottom or in situations in which the wave refraction-diffraction effect is strong.

Due to a lack of field observations and hydraulic experiments regarding the wave refraction/diffraction effects around coastal structures under random wave actions, this research can only evaluate the influences of higher order refraction-diffraction correction parameters from a comparisons between the SWAN model before and after it was modified, and the results show that new version provides more stable numerical results and the new adding correction parameter can affect the results of wave height distribution. However, although the pattern of wave height distribution in both random wave cases seems to be conceptually reasonable, and the original SWAN version has been verified before, more field or experimental data are needed to evaluate the influences from each parameter of the SWAN model.

ACKNOWLEDGMENTS

This research was financially supported by the National Science Council under grant number NSC 97-2221-E-019-047-MY3, Taiwan.

REFERENCES

1. Arthur, R. S., "Refraction of shallow water waves: The combined effects of currents and underwater topography," *EOS Transaction, American Geophysical Union*, Vol. 31, pp. 549-552 (1952).
2. Berkhoff, J. C. W., "Computations of combined refraction, diffraction and reflection," *Proceedings of the 13th International Conference on Coastal Engineering*, ASCE, New York, pp. 471-490 (1972).
3. Booij, N., *Gravity Waves on Water with Non-Uniform Depth and Current*, Ph.D. Thesis, Delft University of Technology, Delft, the Netherlands (1981).
4. Booij, N., Holthuijsen, L. H., Doorn, N., and Kieftenburg, A. T. M. M., "Diffraction in a spectral wave model," *Proceedings of the 3rd International Symposium on Ocean Wave Measurement and Analysis*, WAVES' 97, ASCE, New York, pp. 243-255 (1997).
5. Booij, N., Ris, R. C., and Holthuijsen, L. H., "A third generation wave model for coastal regions: Part I. Model description and validation," *Journal of Geophysical Research*, Vol. 104, No. C4, pp. 7649-7666 (1999).
6. Chamberlain, P. G. and Porter, D., "The modified mild-slope equation," *Journal of Fluid Mechanics*, Vol. 291, pp. 393-407 (1995).
7. Chamberlain, P. G. and Porter, D., "Decomposition methods for wave scattering by topography with application to ripple beds," *Wave Motion*, Vol. 22, pp. 201-214 (1995).
8. Dingemans, M. W., *Surface Wave Propagation over an Uneven Bottom; Evaluation of Two-Dimensional Horizontal Wave Model*, Report W301, Delft Hydraulics (1985).
9. Hasselmann, K., Barnett, T. P., Bouws, E., Carlson, H., Cartwright, D. E., Enke, K., Ewing, J. A., Gienapp, H., Hasselmann, D. E., Kruseman, P., Meerburg, A., Müller, P., Olbers, D. J., Richter, K., Sell, W., and Walden, H., "Measurement of wind-wave growth and swell decay during the Joint North Sea Wave Project (JONSWAP)," *Deutsche Hydrographische Zeitschrift*, Supplement, Series A, No. 12 (1973).
10. Holthuijsen, L. H., Herman, A., and Booij, N., "Phase-decoupled refraction-diffraction for spectral wave models," *Coastal Engineering*, Vol. 49, pp. 291-305 (2003).
11. Hsu, T. W., Ou, S. H., and Liau, J. M., "Hindcasting nearshore wind waves using a FEM code for SWAN," *Coastal Engineering*, Vol. 52, pp. 177-195 (2005).
12. Hsu, T. W. and Wen, C. C., "A parabolic equation extended to take into account rapidly varying topography," *Ocean Engineering*, Vol. 28, pp.

1479-1498 (2001).
13. Hsu, T. W. and Wen, C. C., "On radiation boundary conditions and wave transformation across the surf zone," *China Ocean Engineering*, Vol. 15, No. 3, pp. 395-406 (2001).
14. Ilic, S., van der Westhuysen, A. J., Roelvink, J. A., and Chadwick, A. J., "Multidirectional wave transformation around detached breakwaters," *Coastal Engineering*, Vol. 54, pp. 775-789 (2007).
15. Kirby, J. T., "A note on linear surface wave-current interaction," *Journal of Geophysical Research*, Vol. 89, No. C1, pp. 745-747 (1984).
16. Kirby, J. T., "Higher-order approximation in the parabolic equation method for water waves," *Journal of Geophysical Research*, Vol. 91, No. C1, pp. 933-952 (1986).
17. Liau, J.-M., Roland, A., Hsu, T.-W., Ou, S.-H., and Li, Y.-T., "Wave refraction-diffraction effect in the wind wave model WWM," *Coastal Engineering*, Vol. 58, No. 5, pp. 429-443 (2011).
18. Liu, P. L.-F., "Wave-current interactions on a slowly varying topography," *Journal of Geophysical Research*, Vol. 88, No. C7, pp. 4421-4426 (1983).
19. Liu, P. L.-F., "Wave transformation," in: LeMehaute, B. and Hanes, D. (Eds.), *The Sea: Ocean Engineering Sciences*, Vol. 9, Wiley & Sons (1990).
20. Marcos, F., *Logiciel TOMAWAC de Propagation de Houle En Elements Finis, Notice D'utilisation, Version 5.2*, Chatou, EDF Département Laboratoire National d'Hydrauliqueet Environnement, France (2003).
21. Mase, H., "Mulit-directional random wave transformation model based on energy balance equation," *Coastal Engineering Journal*, Vol. 43, No. 4, pp. 317-337 (2001).
22. Massel, S. R., "Extended refraction-diffraction equation for surface waves," *Coastal Engineering*, Vol. 19, pp. 97-126 (1993).
23. Resio, D. T., "A steady-state wave model for coastal applications," *Proceedings 21st International Conference on Coastal Engineering*, ASCE, New York, pp. 929-940 (1988).
24. Ris, R. C., Holthuijsen, L. H., and Booij, N., "A third-generation wave model for coastal regions: Part 2, Verification," *Journal of Geophysical Research*, Vol. 104, No. C4, pp. 7667-7682 (1999).
25. Rivero, F. J., Arcilla, A. S., and Carci, E., "Analysis of diffraction in spectral wave models," *Proceedings of the 3rd International Symosium on Ocean Wave Measurement and Analysis*, WAVES '97, ASCE, New York, pp. 431-445 (1997).
26. Smith, J. M., Sherlock, A. R., and Resio, D. T., *STWAVE: Steady-State Spectral Wave Model User's Manual for STWAVE, Version 3.0*, Coastal and Hydraulics Laboratory, US Army Corps of Engineers (2001).
27. Smith, R. and Sprinks, T., "Scattering of surface waves by a conical island," *Journal of Fluid Mechanics*, Vol. 72, pp. 373-384 (1975).
28. The SWAN Team, *SWAN User Manual*, Delft University of Technology (2008).
29. The SWAN Team, *SWAN Technical Documentation*, Delft University of Technology (2008).